The Different Nature of Band Edge Absorption and Emission in Colloidal PbSe/CdSe Core/shell Quantum Dots

Bram De Geyter,[†,‡] Yolanda Justo,[†] Iwan Moreels,[†] Karel Lambert,[†] Philippe F. Smet,[¶] Dries Van Thourhout,[‡] Arjan J. Houtepen,[§] Dominika Grodzinska,[‖] Celso de Mello Donega,[‖] Andries Meijerink,[‖] Daniel Vanmaekelbergh,[‖] and Zeger Hens[*,†]

Physics and Chemistry of Nanostructures, Photonics Research Group, Lumilab, Ghent University, Gent, Belgium, Department of Chemistry, Delft University of Technology, Delft, The Netherlands, and Condensed Matter and Interfaces, Debye Institute, Utrecht University, The Netherlands

E-mail: Zeger.Hens@UGent.be

KEYWORDS: semiconductor nanocrystals, core/shell, cation exchange, PbSe/CdSe, oscillator strength, exciton lifetime, exciton absorption, exciton emission

Abstract

We present a quantitative analysis of the absorption and luminescence of colloidal PbSe/CdSe core/shell quantum dots (QDs). In absorption, both the energy and the oscillator strength of

---

[*]To whom correspondence should be addressed
[†]PCN, Ghent University (www.nano.UGent.be)
[‡]Photonics Research Group, Ghent University
[¶]Lumilab, Ghent University
[§]Department of Chemistry, Delft University of Technology
[‖]Condensed Matter and Interfaces, Debye Institute, Utrecht University, The Netherlands

the first exciton transition coincide with that of plain PbSe QDs. In contrast, luminescence lifetime measurements indicate that the oscillator strength of the emitting transition is reduced by at least a factor of 4 compared to PbSe core QDs. Moreover, the addition of an electron scavenger quenches the PbSe/CdSe emission, while a hole scavenger does not. This implies that the electron wavefunction reaches the QD surface, while the hole is confined to the PbSe core. These observations are consistent with calculations based on the effective mass model, which show that PbSe/CdSe QDs are at the boundary between the type-I and quasi-type-II regime, where the electron spreads over the entire nanoparticle and the hole remains confined in the PbSe core. However, as this only leads to a minor reduction of the oscillator strength, it follows that the drastic reduction of the oscillator strength in emission cannot be explained in terms of electron delocalization. In combination with the increased Stokes shift for PbSe/CdSe QDs, this indicates that the emission results from lower energy states that are fundamentally different from the absorbing states.

Compared to plain core quantum dots (QDs), core/shell QDs offer an enhanced stability and tunability of the optical and electronic properties. This difference arises from the spatial distribution of electron and hole wave functions in the QD heterostructures. Based on the bulk band alignment and the effective mass theory in a quantum confined heterostructure, three regimes of core/shell QDs can be distinguished, depending on the localization of the charge carrier wave functions (see Figure 1). In a type-I localization regime, the electron and hole are both localized in the core, resulting in chemically stable and well passivated QDs with high photoluminescence (PL) quantum yield (QY). In a type-II regime the electron and hole are spatially separated. In a quasi-type-II[1] localization regime, one of the carriers is fully delocalized, while the other remains localized. As amply demonstrated with QD heterostructures emitting in the visible, this opens up new possibilities for engineering the intrinsic opto-electronic properties of nanomaterials. For instance, a five-fold reduction of the gain threshold was demonstrated with CdS/ZnSe dots, due to repulsive biexciton interaction of spatially separated excitons.[2] Similar effects, combined with a decrease in the Auger recombination rate were observed for CdTe/CdSe QDs.[3,4] For CdSe/CdTe hetero-nanocrystals[5,6] and ZnTe/ZnSe QDs,[7] long radiative lifetimes, indicative of charge separation,

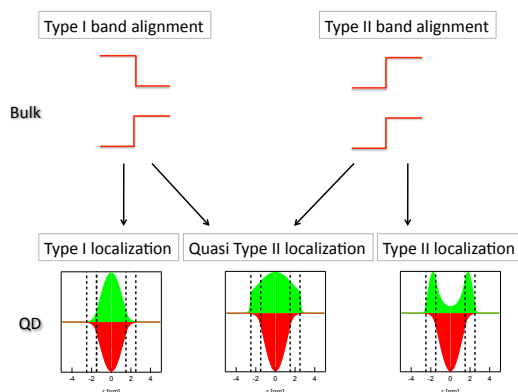and a strong redshift of the exciton transitions were reported.

Figure 1: Core/shell QDs can be divided in three types, depending on the localization of the electron and hole wave function. In type-I, electron and hole are confined in the same region (either core or shell), in type-II, they are spatially separated. In a quasi-type-II one carrier is fully delocalized over the entire volume and one is localized in one region.

Results & Discussion

Previous work on colloidal type-II heteronanocrystals has focused primarily on compositions emitting in the visible spectral range. Colloidal core/shell heterostructures active in the near-infrared wavelength range (1000-3000 nm, NIR) have been scarcely investigated. For example, it has been recently shown that PbSe/PbS core/shell QDs with outer diameters below 10 nm behave like single composition QDs, where electron and hole are delocalized over the entire heterostructure.[8] Colloidal synthesis techniques were recently extended to concentric PbX/CdX (X=S, Se, Te) core/shell QDs.[9,10] In this work we focus on PbSe/CdSe QDs, investigating their carrier distribution by absorption and photoluminescence (PL) spectroscopy and attempt to understand the electronic nature of the lowest absorbing and emitting states.

PbSe/CdSe core/shell QDs were made by cation exchange on PbSe QDs as described by Pietryga *et al.*[9] The cation exchange does not alter the total QD size and original size distribution,[11] and yields PbSe/CdSe core/shell QDs with tunable core size and shell thickness. This is corroborated by the absorption spectra (see Figure 2a), which show an increasing blueshift with

3

increasing exchange time. The blueshift can be attributed to the shrinking of the PbSe core and the simultaneous increase of the CdSe shell thickness. Using high resolution transmission electron microscopy (HR-TEM), we showed that the cation exchange process is quite anisotropic,[11] partially leading to particles with eccentric and non-spherical cores. This heterogeneity accounts for the broadening of the absorption and PL spectra with increasing exchange time (see Figure 2a).
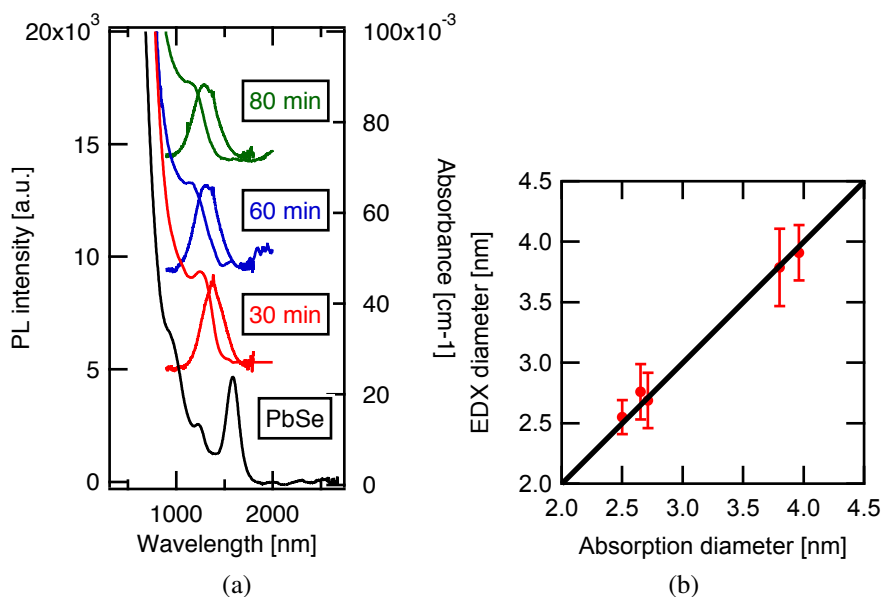

Figure 2: (a) Absorption and luminescence spectra of PbSe/CdSe QDs in C_2Cl_4 for increasing exchange times. (b) Diameter determined from EDX vs. diameter determined from the position of the first absorption peak, using the PbSe sizing curve. The black line indicates a 1-to-1 relationship.[12]

Relation between Absorption Energy and Core Diameter

Knowledge of the core diameter and shell thickness is important for the present study of the QD optical and electronic properties. Although HR-TEM can be used for this purpose, it is not a practical technique for the analysis of a large number of samples in a short time span. Moreover, even when the boundary between core and shell can be distinguished, it is not clear whether to place it on a cation or anion plane. Therefore, we measured the Pb/Se ratio of the original PbSe core QDs and of the derived PbSe/CdSe QDs by TEM-based energy dispersive x-ray spectroscopy (EDX). Since the Se-content stays constant, we can calculate the amount of Pb in the PbSe/CdSe core, taking the

nonstoichiometry[12,13] of the parent PbSe QDs into account (see Supporting Information). Since the stoichiometry of the core is not known, we assume the PbSe core is terminated by Pb-planes and therefore has the stoichiometry of PbSe QD with the same diameter. This effective diameter for the PbSe core, determined with EDX, is in good agreement with the diameter determined using the PbSe QD sizing curve[12] (see Figure 2b). It shows that the Pb content of the PbSe/CdSe QD determines the bandgap and hence we justify using the PbSe QD sizing curve to estimate the PbSe effective core diameter in PbSe/CdSe core/shell QDs.

Absorption Oscillator Strength

The first exciton transition is characterized by its energy and its oscillator strength $f_{if,abs}$. To obtain the oscillator strength, the spectrum of the absorbance (A) must be converted into the spectrum of the molar extinction coefficient ε. For this, the QD concentration c and the cuvette length L are needed (Beer's law):

$$\varepsilon = \frac{A}{cL}$$

Hence, under the assumption that the concentration of PbSe QDs before exchange, which can be calculated from their absorption spectrum,[12] does not change during shell growth, the spectrum of ε is readily obtained from the absorbance spectrum of a PbSe/CdSe suspension.

Having the ε spectrum for PbSe/CdSe QDs with different shell-volume-to-total-QD-volume ratios (V_{sh}/V_{QD}), $f_{if,abs}$ can be calculated from the energy-integrated molar extinction coefficient ε_{gap} of the first exciton transition, in analogy with calculations for PbSe[12] and PbS[16] QDs:

$$f_{if,abs} = \frac{2\epsilon_0 c m_e n_s}{\pi N_A \hbar e} \frac{1}{|f_{LF}|^2} \ln(10) \varepsilon_{gap} \tag{1}$$

Here, ϵ_0 stands for the permittivity of the vacuum, c is the speed of light, m_e the electron mass, n_s the solvent refractive index (1.53 for C_2Cl_4), N_A Avogadro's constant, $\hbar$ Planck's constant, e the unit charge, f_{LF} the local field factor. Neeves et al.[17] provide the following expression for $|f_{LF}|^2$
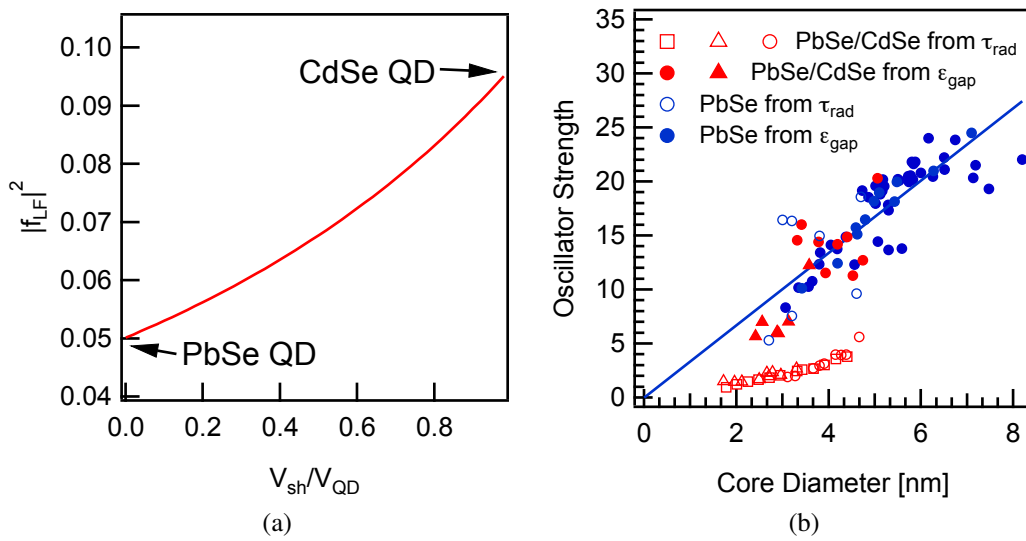
Figure 3: (a) Local field factor at the band edge for PbSe/CdSe QDs as a function of the ratio V_{sh}/V_{QD}. (b) Absorption oscillator strength $f_{if,abs}$ for PbSe QDs (full blue markers) and PbSe/CdSe QDs (full red markers) and emission oscillator strength $f_{if,em}$ for PbSe QDs[14,15] (empty blue markers) and PbSe/CdSe QDs (empty red markers) as a function of the core diameter. The red squares are values for PbSe/CdSe with a total diameter of 6.09 nm, the red dots a total diameter of 5.83 nm and the red triangles a total diameter of 4.57 nm.

The full red curve is a Boltzmann model of the emission oscillator strength for two states separated by the experimentally determined Stokes shift.

in the case of a core/shell particle:

$$|f_{LF}|^2 = \left| \frac{9\varepsilon_{sh}\varepsilon_s}{\varepsilon_{sh}\varepsilon_a + 2\varepsilon_s\varepsilon_b} \right|^2$$

$$with$$

$$\varepsilon_a = \varepsilon_c(3 - 2\frac{V_{sh}}{V_{QD}}) + 2\varepsilon_{sh}\frac{V_{sh}}{V_{QD}}$$

$$\varepsilon_b = \varepsilon_c\frac{V_{sh}}{V_{QD}} + \varepsilon_{sh}(3 - \frac{V_{sh}}{V_{QD}})$$

Using $\varepsilon_c = 25.7$[18] and $\varepsilon_{sh} = 8.3$,[19] we find that $|f_{LF}|^2$ gradually increases from the value for PbSe QDs to the value for CdSe QDs with increasing shell thickness (see Figure 3a). Because of the significant broadening of the first exciton peak at long reaction times, ε_{gap} is obtained by fitting a series of gaussian functions with a polynomial background function to the ε spectrum and taking the area under the first gaussian function (see Supporting Information). The combination of $|f_{LF}|^2$ with the values for ε_{gap} enables us to calculate $f_{if,abs}$ of PbSe/CdSe QDs. Figure 3b shows that in the size range of 2.5 to 5 nm, we obtain similar values as a function of core diameter d_c as for PbSe QDs. This correspondence confirms that the nature of the first absorption feature remains largely unchanged when adding a shell of CdSe.

Steady-state and Time-resolved PL

Next to the absorbance spectrum, Figure 2a shows the PL spectrum for three different suspensions of PbSe/CdSe QDs. Due to the lack of efficient and reliable infrared reference dyes, the quantum yield (QY) is hard to determine. However, we can compare the total emission intensity of oleic acid capped PbSe/CdSe QDs with the total emission intensity of oleic acid capped PbSe QDs,[20] making sure to normalize them relative to the absorbance at the excitation wavelength and keeping all settings of the spectrofluorometer the same. This enables a relative comparison of the QY of different samples, without knowing its exact value. The QY for PbSe/CdSe QDs and PbSe QDs is comparable (see Supporting Information). Although a trend of increasing QY with decreasing core size is present for PbSe/CdSe QDs, the large scatter on these data suggests that sample preparation

and surface quality have a large influence on the observed QY for PbSe/CdSe QDs.

We complemented the steady state PL results with PL lifetime measurements for different samples of PbSe/CdSe QDs, suspended in C_2Cl_4. The steady-state PL spectrum was broadened considerably for all samples to about 250 nm (full width at half maximum). Hence each sample was probed at several wavelengths. Figure 4a shows a typical decay curve for PbSe/CdSe QDs and its PbSe QD parent. From this logarithmic plot, we clearly see that the PbSe QD decay is monoexponential. It is considerably faster than the decay of PbSe/CdSe QDs, which is not monoexponential.

From a single exponential fit to the decay curves of a 4.6 nm PbSe QD sample (see Figure 4a), we obtain an experimental lifetime τ_0 of $0.969 \pm 0.002\,\mu s$, $0.979 \pm 0.002\,\mu s$ and $1.067 \pm 0.002\,\mu s$ respectively at a wavelength of 1375, 1425 and 1500 nm. These results agree with the $1.04\,\mu s$ measured by Kigel *et al.*[15] for 4.7 nm PbSe QDs in chloroform. The decay curves of the different PbSe/CdSe QD samples were fitted with a double exponential, a stretched exponential function and a lognormal distribution of decay rates.[21] The stretched exponential function and the lognormal distribution resulted in a much poorer fit than the double exponential function. For all samples, the double exponential fit yields two decay constants differing by about a factor of 10. However, the intensity (area under decay curve) of the slow decay was 5 to 20 times higher than the intensity of the fast decay. For this reason, we will focus our analysis on the slow component of the decay.

Figure 4b shows the results of the fit procedure (full green squares, open red and blue markers). The lifetime differs significantly for different samples, ranging from 1.5 to 7 μs. The fact that PbSe/CdSe QDs from different suspensions, yet with comparable core diameters and shell thicknesses yield strongly different lifetimes suggests that the experimental lifetime τ_0 depends on the QY of each sample. In that case, the radiative lifetime τ_{rad} follows from:

$$\tau_0 = (\tau_{rad}^{-1} + \tau_{nrad}^{-1})^{-1} = \tau_{rad}QY \tag{2}$$

Since we are not able to determine the absolute QY, we cannot determine the τ_{rad} of the QDs.

However, the relative QY allows us to rescale the values of τ_0, so we can compare the lifetimes of different QD suspensions. In Figure 4b the arrows illustrate that by rescaling the lifetime of each of the open red and open blue markers to the QY of the sample with full green squares, we obtain a one-to-one relation between core size and lifetime. We note that these values, between 4 and 7 μs, are a lower limit of τ_{rad}. From Figure 4b, we see that the lifetime decreases with increasing core diameter. This was predicted by Moreels *et al.*[16] using the molar extinction coefficient at the band gap for PbSe QDs up to 5 nm. Kigel *et al.*[15] measured a similar decreasing trend. For all wavelengths, the values are at least 4 to 6 times higher for PbSe/CdSe QDs than for PbSe QDs. [14,15,22]
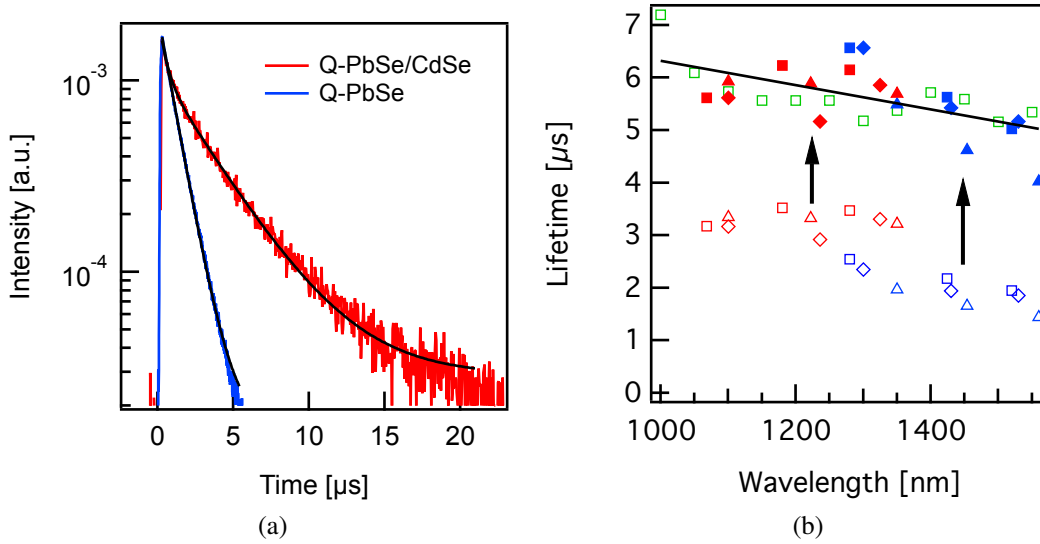

(a)   (b)

Figure 4: (a) Typical decay curve for PbSe/CdSe QDs and their PbSe QD parent, shown on a logarithmic scale. A single exponential fit is shown for PbSe and a biexponential fit for PbSe/CdSe. (b) Lifetime for 7 samples of PbSe/CdSe QDs. Each sample is probed at different wavelengths (markers with equal colour and symbol). Green squares have a PbSe QD parent diameter of 6.09 nm, blue markers a PbSe QD parent diameter of 5.83 nm and red markers a parent diameter of 4.57 nm. Open symbols give the decay constant for the slow component obtained from a bi-exponential fit to experimental decay curves. Closed symbols give the fitted values rescaled according to the QY of each individual sample, taking the sample with open green squares as the standard.

From the lower limit of the radiative lifetime obtained above for PbSe/CdSe QDs and literature values for PbSe QDs, [14,15] we can calculate an upper limit of the oscillator strength $f_{if,PbSe/CdSe,em}$

and $f_{if,PbSe,em}$ of the emitting transition.

$$f_{if,em} = \frac{2\pi\epsilon_0 c^3 m_e}{e^2} \frac{g}{n_s |f_{LF}|^2 \omega^2} \tau_{rad}^{-1} \tag{3}$$

Dielectric screening will affect the radiative lifetime. Therefore we correct for this local field effect with f_{LF}. While the absorption oscillator strength is the sum of the transition strengths of all exciton states f_k:

$$f_{if,abs} = \sum_{k=1}^{g} f_k \tag{4}$$

the emission oscillator strength is, taking into account possible splitting between the states, a Boltzmann weighted average of the transition strength of each exciton state:[23]

$$f_{if,em} = g \frac{\sum_{k=1}^{g} f_k e^{\frac{-\Delta E_k}{kT}}}{\sum_{k=1}^{g} e^{\frac{-\Delta E_k}{kT}}} \tag{5}$$

Effectively, this yields the average transition strength of the states that contribute to emission. Since emission comes from radiative decay of a single exciton, which occupies only one of all possible ground exciton states, and absorption involves all exciton states, we multiply in Eq. (5) by the total number of exciton states $g = 64$ to obtain a total emission oscillator strength. This is equivalent to compressing the fine structure to one single emitting state with degeneracy g and oscillator strength $f_{if,em}$.

The resulting values for $f_{if,PbSe/CdSe,em}$ and $f_{if,PbSe,em}$ are represented by the open markers in red and blue respectively in Figure 3b. The values for $f_{if,PbSe,em}$ are similar to the values obtained from the absorption spectrum $f_{if,PbSe,abs}$. Values smaller by at least 75% are found for the emission oscillator strength $f_{if,PbSe/CdSe,em}$.

PL Quenching

The quantitative analysis of the absorption and luminescence data yields contradictory outcomes. While the energy and the absorption oscillator strength of the band gap transition in PbSe/CdSe
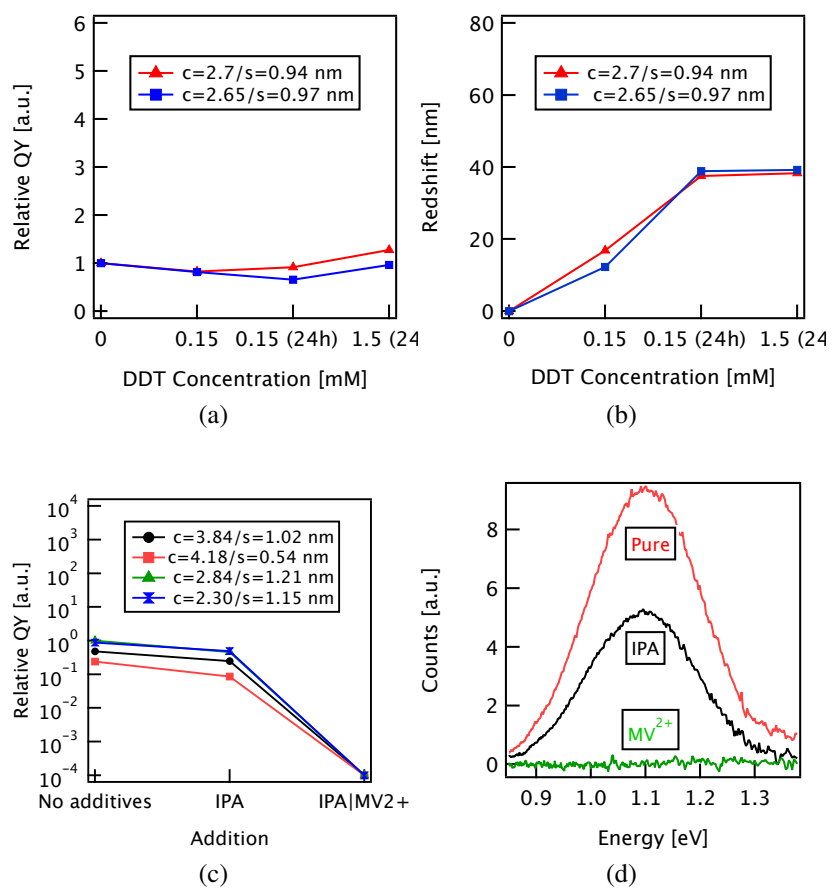
Figure 5: (a) Relative QY and (b) PL redshift before and after adding thiols (c) Relative QY (log-scale) and (d) PL spectra before and after adding IPA and MV^{2+}/IPA.

are indicative of a type-I localization regime, the sensitivity of the emission QY and the increase in exciton lifetime associated with a decrease in emission oscillator strength suggest that one of the carriers is delocalized over the entire QD (quasi-type-II) or even localized in the CdSe shell (type-II). To pinpoint the localization regime, we added dodecanethiol (DDT), a well-known hole scavenger for CdSe[24,25] and PbSe[26,27] and methyl viologen (MV^{2+}), an electron scavenger,[28,29] to PbSe/CdSe suspensions and analyzed their effect on the photoluminescence.

Adding DDT ($150\mu M$) to a PbSe/CdSe suspension (see Supporting Information) does not affect the QY (Figure 5a). It redshifts the emission spectra by 20-40 nm (see Figure 5b), indicating interaction of at least one of the charge carriers with the surface.[30,31] In contrast, addition of DDT to a PbSe QD sample resulted in significant quenching of the PL. Methylviologen dichloride was dissolved in isopropanol (IPA) and the MV^{2+}/IPA mixture was added in a 1:33 (v:v) ratio to obtain a $150\mu M$ MV^{2+} concentration. As a reference, we added the same amount of pure IPA to an identical QD sample, which resulted in a 50% drop of the QY. Adding the MV^{2+} mixture however immediately quenches the PL signal to values below the detection limit (Figure 5c and Figure 5d). The same result was obtained for a PbSe QD reference sample. This shows that PbSe/CdSe QDs emit from a state in which the electron wave function reaches the surface and the hole wave function is well confined to the core. It confirms that PbSe/CdSe are in the (quasi)-type-II localization regime. The delocalization of the electron will reduce the wavefunction overlap to some extent. However, these measurements are not sufficient to conclude that this reduction in overlap fully accounts for the reduction in emission oscillator strength. In addition, they do not explain why the absorption oscillator strength essentially remains unchanged.

Table 1: Effective masses of PbSe and cubic CdSe.

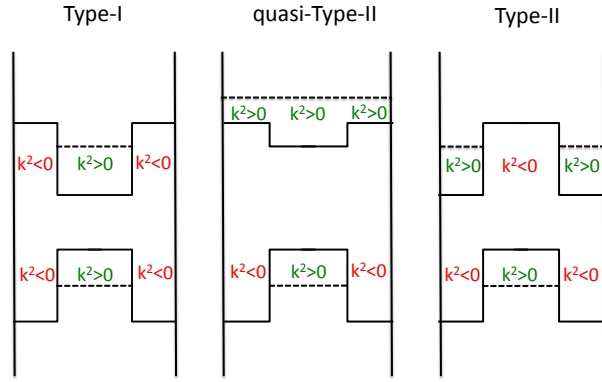|	PbSe[32]	cubic CdSe[33,34]
m_e	0.047	0.12
m_h	0.040	0.8

Effective Mass Modelling

Atomistic calculations that reconcile the experimental results are not yet available. Therefore, we interpret our results in terms of an effective mass model, based on literature data of the bulk band alignment and the effective masses.[32–34] In addition, we use the energy criterion introduced by Klimov *et al.* to classify quantum confined heterojunctions based on their carrier localization.[35] This criterion can best be appreciated by means of the square of the wavenumber for electron (k_e^2) and hole (k_h^2):
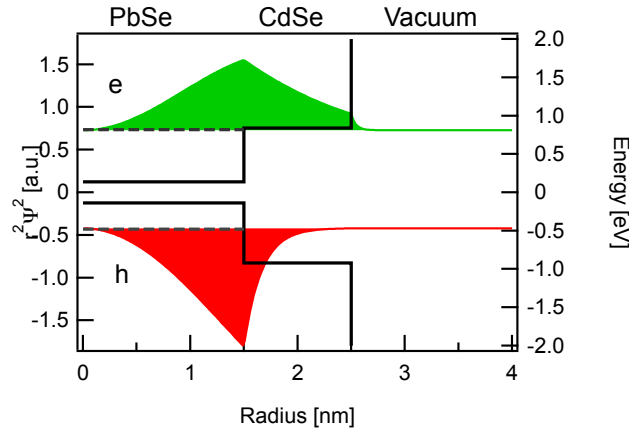
$$k_{e,h}^2 = \frac{2m_{e,h}}{\hbar^2}(E_{e,h} - V_{e,h})$$

Here, $V_{e,h}$ denotes the potential (i.e., the position of the bulk energy bands) in each region and $m_{e,h}$ the effective mass for electron and hole. If k^2 is negative, the wavenumber is imaginary, resulting in an exponentially decaying wave function. Provided that the characteristic decay length k^{-1} is sufficiently small, this means that a charge carrier is preferentially found in that region of the heterostructure where k^2 is positive and the resulting wave number is real. Hence, looking at binary heterostructures, we talk about type-I regime, if k_e^2 and k_h^2 have the same sign in each region of the heterostructure. For type-II regime, k_e^2 and k_h^2 have opposite sign in every region. Finally, for quasi-type-II regime, k_e^2 and k_h^2 have the same sign in one of the regions, and opposite sign in the other region (see Figure 6a).
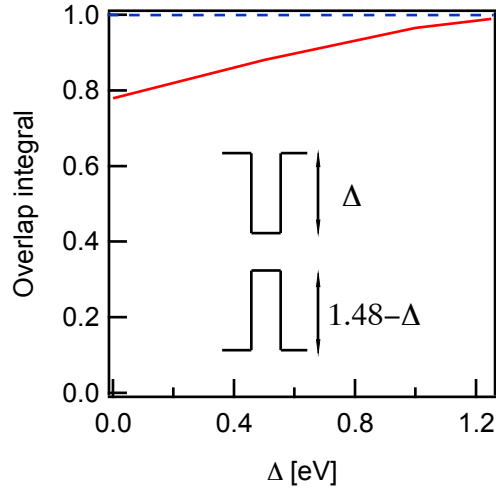
According to Michaelson,[36] bulk PbSe and CdSe have a type-I bulk band alignment with a valence band offset of 0.78 eV and conduction band offset of 0.70 eV. Using the effective masses of PbSe and CdSe as summarized in Table 1, we obtain the wave function of a PbSe/CdSe QD with a core radius of 1.5 nm and a shell thickness 1 nm as plotted in Figure 6b. Due to the difference in effective mass between electron and hole in CdSe, we find that the electron wave function spreads throughout the entire QD, while the hole wave function is confined to the core. Taking the band offset Δ as an adjustable parameter, we find that PbSe/CdSe QDs are at the boundary between the type-I and quasi-type-II regime. The overlap integral slightly drops from a value close to one for large band offsets to about 0.8 when Δ equals zero. Since the overlap integral is directly

(a)

(b)

(c)

Figure 6: (a) Definition of types of localization regimes in core/shell quantum dots in terms of the square of the wavenumber k^2. (b) Electron and hole wave functions ($r^2\Psi^2$) for PbSe/CdSe QDs (green and red) in a simple effective mass model. The confinement energy (striped) is drawn within the bulk band diagram. (c) Overlap integral as a function of the conduction band offset Δ. The dotted line shows the overlap integral for PbSe QDs.

14

proportional to the oscillator strength, this confirms the experimental result that $f_{if,PbSe/CdSe,abs}$ does not significantly differ from $f_{if,PbSe,abs}$.

Eventhough there is only a small reduction in overlap, the electron wavefunction does have a non-zero value at the QD outer surface, while the hole wavefunction is negligible at the QD outer surface. This overall picture is confirmed by the PL quenching experiments, which show that the electron is transferred to the electron acceptor at the surface, while the hole does not transfer to the hole acceptor.

This simple model fails to explain why $f_{if,PbSe/CdSe,em}$ is reduced. The fact that the QY of PbSe/CdSe QDs is comparable to and often higher than that of PbSe QDs and the clear dependence of $f_{if,PbSe/CdSe,em}$ on the QD diameter indicate that this is most likely an intrinsic PbSe/CdSe QD property, and not an artefact due to surface-state mediated radiative recombination. Therefore, it suggests that the fine structure of PbSe/CdSe QDs, which our model cannot resolve, is more complex. Looking at Eq. (4) and Eq. (5), $f_{if,abs}$ and $f_{if,em}$ will only differ significantly, when (a) the energy splitting is much larger than the thermal energy kT and (b) the emitting states have a much lower oscillator strength than the absorbing states. Therefore, the band edge emission in PbSe/CdSe QDs comes from states, that are fundamentally different from the bright absorbing states.

Stokes shift

A splitting of the band edge in a lower energy dark and higher energy bright state due to the exchange interaction was predicted for PbSe QDs by An *et al.*[23] This so-called exchange splitting however is only between 0 and 20 meV. Hence, at room-temperature these states are both populated due to thermal excitation, resulting in similar values for $f_{if,PbSe,abs}$ and $f_{if,PbSe,em}$. According to An *et al.*,[23] the exchange splitting, together with the intervalley splitting, explains the non-resonant Stokes shift in PbSe QDs. Figure 6 shows the Stokes shift of PbSe QDs (blue squares) and PbSe/CdSe QDs (red dots) as a function of absorption energy or core size. Our values for PbSe QDs extrapolate well to the theoretical values reported for small QDs.[23,37,38]

Like the band gap energy, the PbSe/CdSe QD Stokes shift depends only on the core size, but it exceeds that for PbSe QDs by 50 to 100 meV. For small cores, it reaches a value of 200 meV. The molar extinction coefficient at energies well above the bandgap is typically volume dependent for colloidal QDs. Therefore a broad size distribution can result in a shift in the PL spectrum, because larger particles are excited more than smaller particles. For PbSe/CdSe QDs, we recently showed that the molar extinction coefficient is largely dependent on the total QD volume.[39] Since the total volume and total size dispersion remain constant for these QDs throughout the exchange procedure,[9] we expect an increase in the Stokes shift due to non-uniform excitation of maximum 10 meV for the most broadened sample. The large Stokes shift is therefore not an artefact of size broadening, but due to an intrinsic physical effect. Increased splitting in the fine structure will according to Boltzmann statistics result in an increased Stokes shift. Hence, it confirms that the band edge emission results mostly from lower energy states with reduced oscillator strength as compared to the higher energy absorbing states.

This fine structure cannot be understood without extensive modelling. The nature of the interface, both in the real and in the reciprocal lattice (the band edge states are around the L-point for PbSe and the Γ-point for CdSe) probably has a strong influence on the electronic properties of these heterostructures. This could result in increased exchange and intervalley splitting, or might induce states at the PbSe/CdSe interface. For PbTe/CdTe however, theoretical calculations did not yield such interfacial states,[40] because the atomic structure of the lattice at the interface is virtually unperturbed.

Our results indicate that PbSe/CdSe QDs might have potential for applications in near infrared light sources, provided that further theoretical and experimental work reveals more of the intrinsic physical properties. In PbSe QDs the multi-exciton emission from the band edge, which at room temperature is essentially 8-fold degenerate, competes with the ps non-radiative Auger process. In PbSe/CdSe QDs, the emission comes mainly from lower energy states with much lower oscillator strength. If these states are non-degenerate, like the lowest dark state of PbSe,[23] it would allow population inversion with less than one exciton per QD. This could mean a reduction in the
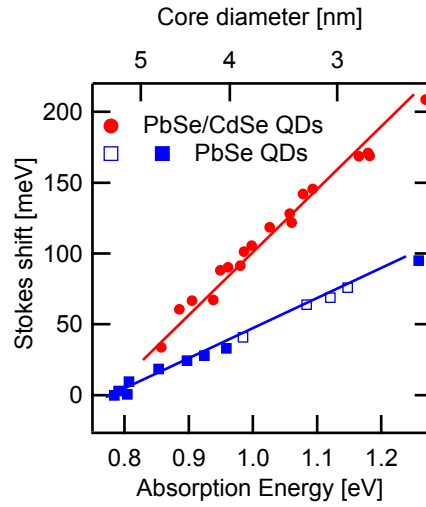
continuous wave lasing threshold of up to 10^{-4}.

Figure 7: Stokes shift for PbSe QD (full and open[15] blue squares)

Conclusion

In conclusion, we show that both the energy and the absorption oscillator strength of the first absorption peak in PbSe/CdSe quantum dots follow the same trend with core diameter as PbSe QDs. On the other hand, PL lifetime measurements yield an oscillator strength in emission that is reduced by at least 75%, compared to the PbSe/CdSe oscillator strength from absorption and the PbSe QD oscillator strength in absorption and emission. Moreover, the addition of an electron scavenger leads to a complete quenching of the PbSe/CdSe QD PL, while a hole scavenger does not. These results can be rationalized by an effective mass model that depicts a PbSe/CdSe QD as a quantum confined heterostructure at the boundary between a type-I and a quasi-type-II localization regime. They show that the absorbing states essentially remain unchanged by the addition of a CdSe shell. However, they do not explain the reduction of the oscillator strength of the band gap emission. In combination with the significantly increased Stokes shift, we conclude that the band gap emission in PbSe/CdSe QDs comes from fundamentally different states with lower oscillator strength that are energetically well separated from the absorbing states at room temperature. Moreover, these

17

emitting states are different than the emitting states in PbSe QDs. Depending on the degeneracy of the emitting states, these binary heterostructures could allow lasing in the NIR wavelength range using single excitons.

Methods

Materials

Technical oleic acid (90%) was purchased from Sigma-Aldrich. PbCl2 (99.999%), PbO (99.999%), Selenium powder (-200 mesh, 99.999%) were ordered from Alfa-Aesar. CdO (99.999%) and Tri-n-octylphosphine (97%) were obtained from Strem Chemicals. Diphenyl ether, methanol, butanol, and toluene were all of quality "for synthesis" and were ordered from VWR.

PbSe synthesis

Monodisperse colloidal PbSe QDs were synthesized by a high-temperature synthesis developed by Murray *et al.*[41] The ligand shell consists of oleic acid (OA), as shown by nuclear magnetic resonance spectroscopy.[20]

PbSe/CdSe cation exchange

PbSe/CdSe core-shell QDs were synthesized starting from PbSe core QDs by means of a cation exchange reaction.[9] In this reaction, Cd-oleate (0.3M stock solution) is added to a PbSe QD suspension in toluene at 100°C (the typical Pb:Cd ratio used is 1:10). After 40 minutes, the reaction is quenched using a mixture of MeOH and BuOH (1:2) and precipitated twice.

Determination of the core diameter and concentration

The absorbance spectra are measured with a Perkin-Elmer Lambda 950 UV/VIS/NIR spectrophotometer. We use a black walled self-masking microcell with a path length of $l = 1$ cm. The

absorption diameter is determined from the spectral position of the first absorption peak and the PbSe sizing curve.[12] For the determination of ε, care is taken to recover all QD material from the cation exchange step and resuspend the resulting PbSe/CdSe core/shell QDs in the same volume. We assume the concentration of this suspension to be identical to the concentration of the PbSe QD parent suspension. Equal volumes are then taken, dried and dissolved in C_2Cl_4 to measure the absorbance A. After converting the absorption spectrum to a molar extinction coefficient spectrum, the first peak was integrated on an energy scale between the low energy onset of the first absorption peak and the maximum of first absorption peak. This value was doubled to obtain the values for ε_{gap}.

Steady-state PL

The steady state PL is measured using an Edinburgh Instruments FS920 PL setup and excited at 400 nm using a 500W Xenon lamp, coupled to a monochromator. The PL is measured using a liquid N_2 cooled Ge detector, coupled to a monochromator. The PL spectra are corrected for detector and grating efficiency. The absorbance at 400 nm is kept below 0.1 cm^{-1} to avoid inhomogeneous spatial excitation and reabsorption. For more information on the determination of the relative QY, we refer to the Supporting Information.

Time-resolved PL

Luminescence decay curves were recorded under pulsed excitation with a Spectra-Physik LPD3000 dye laser at 480 nm pumped by a Lambda Physik LPX excimer laser. The Multi Channel Scaling (MCS) option integrated in the FLS920 spectrofluorometer was used to record the luminescence decay curves, using the IR-sensitive Hamamatsu R5509-72 photomultiplier tube. We measured 7 different PbSe/CdSe samples in C_2Cl_4. The samples stemmed from three PbSe QD parent suspensions with diameter of 4.6 nm, 5.8 nm and 6.1 nm. The core diameters ranged between 2.5 and 4.2 nm. The average shell thickness was between 0.8 and 1.4 nm. With the lattice constant of cubic CdSe (0.6077 nm), this is between 2 and 4 monolayers of CdSe.

Determination of the Stokes shift

The PL spectrum was converted to an energy scale with the appropriate correction and fitted using a gaussian curve. The absorption spectrum was fitted on an energy scale using a gaussian curve and a polynomial background function. The Stokes shift was determined as the difference between the absorption energy and the luminescence energy from the fitting procedures.

Acknowledgement

References

1. Ivanov, S. A.; Piryatinski, A.; Nanda, J.; Tretiak, S.; Zavadil, K. R.; Wallace, W. O.; Werder, D.; Klimov, V. I. Type-Ii Core/Shell Cds/Znse Nanocrystals: Synthesis, Electronic Structures, and Spectroscopic Properties. *J. Am. Chem. Soc.* **2007**, *129*, 11708–11719.

2. Klimov, V. I.; Ivanov, S. A.; Nanda, J.; Achermann, M.; Bezel, I.; McGuire, J. A.; Piryatinski, A. Single-Exciton Optical Gain in Semiconductor Nanocrystals. *Nature* **2007**, *447*, 441–446.

3. Oron, D.; Kazes, M.; Banin, U. Multiexcitons in Type-II Colloidal Semiconductor Quantum Dots. *Phys. Rev. B* **2007**, *75*, 035330.

4. Dorfs, D.; Franzl, T.; Osovsky, R.; Brumer, M.; Lifshitz, E.; Klar, T. A.; Eychmueller, A. Type-I and Type-II Nanoscale Heterostructures Based on CdTe Nanocrystals: A Comparative Study. *Small* **2008**, *4*, 1148–1152.

5. Jones, M.; Kumar, S.; Lo, S. S.; Scholes, G. D. Exciton Trapping and Recombination in Type II CdSe/CdTe Nanorod Heterostructures. *J. Phys. Chem. C* **2008**, *112*, 5423–5431.

6. de Mello Donegá, C. Formation of Nanoscale Spatially Indirect Excitons: Evolution of the Type-II Optical Character of CdTe/CdSe Heteronanocrystals. *Phys. Rev. B* **2010**, *81*, 165303.

7. Bang, J.; Park, J.; Lee, J. H.; Won, N.; Nam, J.; Lim, J.; Chang, B. Y.; Lee, H. J.; Chon, B.; Shin, J. et al. ZnTe/ZnSe (Core/Shell) Type-II Quantum Dots: Their Optical and Photovoltaic Properties. *Chem. Mater.* **2010**, *22*, 233–240.

8. Bartnik, A. C.; Wise, F. W.; Kigel, A.; Lifshitz, E. Electronic Structure of PbSe/PbS Core-Shell Quantum Dots. *Phys. Rev. B* **2007**, *75*, 245424.

9. Pietryga, J.; Werder, D.; Williams, D.; Casson, J.; Schaller, R.; Klimov, V.; Hollingworth, J. Utilizing the Lability of Lead Selenide to Produce Heterostructured Nanocrystals with Bright, Stable Infrared Emission. *J. Am. Chem. Soc.* **2008**, *130*, 4879–4885.

10. Zhang, Y.; Dai, Q.; Li, X.; Cui, Q.; Gu, Z.; Zou, B.; Wang, Y.; Yu, W. W. Formation of PbSe/CdSe Core/Shell Nanocrystals for Stable Near-Infrared High Photoluminescence Emission. *Nanoscale Res. Lett.* **2010**, *5*, 1279–1283.

11. Lambert, K.; De Geyter, B.; Moreels, I.; Hens, Z. PbTelCdTe CorelShell Particles by Cation Exchange, a HR-TEM study. *Chem. Mater.* **2009**, *21*, 778–780.

12. Moreels, I.; Lambert, K.; De Muynck, D.; Vanhaecke, F.; Poelman, D.; Martins, J. C.; Allan, G.; Hens, Z. Composition and Size-Dependent Extinction Coefficient of Colloidal PbSe Quantum Dots. *Chem. Mater.* **2007**, *19*, 6101–6106.

13. Dai, Q.; Wang, Y.; Li, X.; Zhang, Y.; Pellegrino, D. J.; Zhao, M.; Zou, B.; Seo, J.; Wang, Y.; Yu, W. W. Size-Dependent Composition and Molar Extinction Coefficient of PbSe Semiconductor Nanocrystals. *ACS Nano* **2009**, *3*, 1518–1524.

14. Schaller, R. D.; Crooker, S. A.; Bussian, D. A.; Pietryga, J. M.; Joo, J.; Klimov, V. I. Revealing the Exciton Fine Structure of PbSe Nanocrystal Quantum Dots Using Optical Spectroscopy in High Magnetic Fields. *Phys. Rev. Lett.* **2010**, *105*, 067403.

15. Kigel, A.; Brumer, M.; Maikov, G. I.; Sashchiuk, A.; Lifshitz, E. Thermally Activated Photoluminescence in Lead Selenide Colloidal Quantum Dots. *Small* **2009**, *5*, 1675–1681.

16. Moreels, I.; Lambert, K.; Smeets, D.; De Muynck, D.; Nollet, T.; Martins, J. C.; Vanhaecke, F.; Vantomme, A.; Delerue, C.; Allan, G. et al. Size-Dependent Optical Properties of Colloidal PbS Quantum Dots. *ACS Nano* **2009**, *3*, 3023–3030.

17. Neeves, A.; Birnboim, M. Composite Structures for the Enhancement of Nonlinear-Optical Susceptibility. *J. Opt. Soc. Am. B* **1989**, *6*, 787–796.

18. Suzuki, N.; Sawai, K.; Adachi, S. Optical Properties of PbSe. *J. Appl. Phys.* **1995**, *77*, 1249–1255.

19. Ninomiya, S.; Adachi, S. Optical Properties of Cubic and Hexagonal Cdse. *J. Appl. Phys.* **1995**, *78*, 4681–4689.

20. Moreels, I.; Fritzinger, B.; Martins, J. C.; Hens, Z. Surface Chemistry of Colloidal PbSe Nanocrystals. *J. Am. Chem. Soc.* **2008**, *130*, 15081–15086.

21. van Driel, A. F.; Nikolaev, I. S.; Vergeer, P.; Lodahl, P.; Vanmaekelbergh, D.; Vos, W. L. Statistical Analysis of Time-Resolved Emission from Ensembles of Semiconductor Quantum Dots: Interpretation of Exponential Decay Models. *Phys. Rev. B* **2007**, *75*, 035329.

22. Oron, D.; Aharoni, A.; Donega, C. d. M.; van Rijssel, J.; Meijerink, A.; Banin, U. Universal Role of Discrete Acoustic Phonons in the Low-Temperature Optical Emission of Colloidal Quantum Dots. *Phys. Rev. Lett.* **2009**, *102*, 177402.

23. An, J. M.; Franceschetti, A.; Zunger, A. The Excitonic Exchange Splitting and Radiative Lifetime in Pbse Quantum Dots. *Nano Lett.* **2007**, *7*, 2129–2135.

24. Aldana, J.; Wang, Y.; Peng, X. Photochemical Instability of CdSe Nanocrystals Coated by Hydrophilic Thiols. *J. Am. Chem. Soc.* **2001**, *123*, 8844–8850.

25. Wuister, S. F.; Donega, C. D.; Meijerink, A. Influence of Thiol Capping on the Exciton Luminescence and Decay Kinetics of CdTe and CdSe Quantum. *J. Phys. Chem. B* **2004**, *108*, 17393–17397.

26. Wang, C.; Kwon, K.-W.; Odlyzko, M. L.; Lee, B. H.; Shim, M. Pbse Nanocrystal/TiOx Heterostructured Films: A Simple Route to Nanoscale Heterointerfaces and Photocatalysis. *J. Phys. Chem. C* **2007**, *111*, 11734–11741.

27. Luther, J. M.; Law, M.; Song, Q.; Perkins, C. L.; Beard, M. C.; Nozik, A. J. Structural, Optical, and Electrical Properties of Self-Assembled Films of PbSe Nanocrystals Treated with 1,2-Ethanedithiol. *ACS Nano* **2008**, *2*, 271–280.

28. Burda, C.; Green, T.; Link, S.; El-Sayed, M. Electron Shuttling across the Interface of Cdse Nanoparticles Monitored by Femtosecond Laser Spectroscopy. *J. Phys. Chem. B* **1999**, *103*, 1783–1788.

29. Matylitsky, V. V.; Dworak, L.; Breus, V. V.; Basche, T.; Wachtveitl, J. Ultrafast Charge Separation in Multiexcited CdSe Quantum Dots Mediated by Adsorbed Electron Acceptors. *J. Am. Chem. Soc.* **2009**, *131*, 2424–2425.

30. Koole, R.; Luigjes, B.; Tachiya, M.; Pool, R.; Vlugt, T. J. H.; Donega, C. D. M.; Meijerink, A.; Vanmaekelbergh, D. Differences in Cross-Link Chemistry between Rigid and Flexible Dithiol Molecules Revealed by Optical Studies of CdTe Quantum Dots. *J. Phys. Chem. C* **2007**, *111*, 11208–11215.

31. Talgorn, E.; Moysidou, E.; Abellon, R. D.; Savenije, T. J.; Goossens, A.; Houtepen, A. J.; Siebbeles, L. D. A. Highly Photoconductive CdSe Quantum-Dot Films: Influence of Capping Molecules and Film Preparation Procedure. *J. Phys. Chem. C* **2010**, *114*, 3441–3447.

32. Martinez, G.; Schlüter, M.; Cohen, M. L. Electronic Structure of PbSe and PbTe. I. Band Structures, Densities of States, and Effective Masses. *Phys. Rev. B* **1975**, *11*, 651–659.

33. Dalven, R. Calculation of Effective Masses in Cubic CdS and CdSe. *Phys. Status Solidi B* **1971**, *48*, K13.

34. Nikitine, S.; Dimmock, J.; Wheeler, R. Exciton Structure and Zeeman Effects in Cadmium Selenide. *J. Appl. Phys.* **1961**, *32*, 2271–2277.

35. Piryatinski, A.; Ivanov, S. A.; Tretiak, S.; Klimov, V. I. Effect of Quantum and Dielectric Confinement on the Exciton-Exciton Interaction Energy in Type II Core/Shell Semiconductor Nanocrystals. *Nano Lett.* **2007**, *7*, 108–115.

36. Michaelson, H. B. Relation between an Atomic Electronegativity Scale and the Work Function. *IBM J. Res. Dev.* **1978**, *22*, 72–80.

37. Leitsmann, R.; Bechstedt, F. Characteristic Energies and Shifts in Optical Spectra of Colloidal IV-VI Semiconductor Nanocrystals. *ACS Nano* **2009**, *3*, 3505–3512.

38. Franceschetti, A. Structural and Electronic Properties of PbSe Nanocrystals from First Principles. *Phys. Rev. B* **2008**, *78*, 075418.

39. De Geyter, B.; Hens, Z. The Absorption Coefficient of PbSe/CdSe Core/shell Colloidal Quantum Dots. *Appl. Phys. Lett.* **2010**, *97*, 161908.

40. Leitsmann, R.; Bechstedt, F.; Groiss, H.; Schaeffler, F.; Heiss, W.; Koike, K.; Harada, H.; Yano, M. Structural and Electronic Properties of PbTe (Rocksalt)/CdTe (Zinc-Blende) Interfaces. *Appl. Surf. Sci.* **2007**, *254*, 397–400.

41. Murray, C.; Sun, S.; Gaschler, W.; Doyle, H.; Betley, T.; Kagan, C. Colloidal Synthesis of Nanocrystals and Nanocrystal Superlattices. *IBM J. Res. Dev.* **2001**, *45*, 47–56.

Supporting Information Available

Techniques used for calculation of the size from EDX, the QY and Stokes shift. Fits to the absorption spectrum, along with fitting data. Details on the effective mass model.

This material is available free of charge via the Internet at `http://pubs.acs.org/`.

Graphical TOC Entry